ARTICLES
PUBLISHED ONLINE: 8 JULY 2012 | DOI: 10.1038/NPHYS2362
nature physics

# Commensurability and chaos in magnetic vortex oscillations

Sebastien Petit-Watelot[1,2], Joo-Von Kim[1,2]*, Antonio Ruotolo[3,4], Ruben M. Otxoa[1,2], Karim Bouzehouane[3], Julie Grollier[3], Arne Vansteenkiste[5], Ben Van de Wiele[6], Vincent Cros[3] and Thibaut Devolder[1,2]

**Magnetic vortex dynamics in thin films is characterized by gyrotropic motion, the sense of gyration depending on the vortex core polarity, which reverses when a critical velocity is reached. Although self-sustained vortex oscillations in nanoscale systems are known to be possible, the precise role of core reversal in such dynamics remains unknown. Here we report on an experimental observation of periodic core reversal during self-sustained vortex gyration in a magnetic nanocontact system. By tuning the ratio between the gyration frequency and the rate of core reversal, we show that commensurate phase-locked and incommensurate chaotic states are possible, resulting in Devil's staircases with driving currents. These systems could have the potential to serve as tunable nanoscale radiofrequency electrical oscillators for secure communications, allowing schemes such as encryption by chaos on demand.**

Vortices in magnetic thin films represent a configuration of magnetic moments, resulting from competing exchange and dipolar interactions, in which magnetization curls in the film plane and culminates out of the plane at the centre of the vortex core[1]. The core is compact, typically tens of nanometres wide, and its dynamics involves damped gyrotropic motion in the film plane. The gyration frequency depends on the magnetic potential energy, whereas the sense of gyration is determined by the vortex core polarity $p$, which describes the handedness of the magnetization state[2].

Steady-state gyration is possible by means of resonant excitation, for example, by driving the system with alternating magnetic fields[3,4] or currents[5], or by compensating intrinsic energy losses due to magnetic damping, for example, through spin transfer torques[6–10], leading to self-sustained oscillations. In the latter, the torques originate from the exchange interaction between magnetization and a spin-polarized electrical current, which occurs in multilayers[11,12] and continuous systems in which magnetization gradients exist[13,14]. The compact nature of the core, combined with the tunability in the gyration frequency afforded by applied currents and fields, underpins many recent proposals for nanoscale radiofrequency oscillators based on magnetic vortices.

An example of spin-torque-driven vortex oscillations occurs in magnetic nanocontacts[6–8]. In these systems, the large current densities required for spin torques are attained by passing an electrical current into an extended spin valve through a metallic point contact, typically tens of nanometres in size (Fig. 1a). Although the currents flowing through and underneath the nanocontact are largely perpendicular to the film plane, only in-plane components survive farther from the nanocontact owing to the way electrical contacts are made[15]. The perpendicular currents generate a large Oersted–Ampère field with a circulating configuration around the nanocontact, which favours a vortex state in the free magnetic layer through the Zeeman interaction. This interaction also generates a confining potential for the core, whose minimum is centred about the nanocontact. For electron flow away from the nanocontact ($I > 0$), spin torques associated with in-plane currents[14] drive the vortex core away from the nanocontact, whereas magnetic damping leads to motion of the core towards the nanocontact centre. As a result of these competing forces, self-sustained vortex gyration around the nanocontact can take place (Fig. 1b). Unlike dynamics in nanopillars in which vortex motion is physically constrained, these steady-state orbits can reach a few hundred nanometres and occur outside the nanocontact region itself[7]. In such cases the, free-layer magnetization remains largely uniform under the contact and rotates with the vortex gyration, leading to an appreciable time-varying giant magnetoresistance (GMR) signal.

One unexplored aspect of large-orbit oscillations is the critical core velocity. When this value is attained, the core magnetization switches its orientation through a process of vortex–antivortex pair creation and annihilation[5,16,17], resulting in energy dissipation through spin waves[18]. This occurs because the core becomes deformed as it moves, developing a dip structure in which magnetization is oriented antiparallel to the core polarity[19,20], and this deformation develops an instability when the critical velocity is reached. Furthermore, this dip is amplified in the presence of in-plane currents[21]. Although core switching can be initiated by resonant a.c. electrical currents[5], tailored microwave field pulses[22,23] or spin waves[24], its occurrence in self-sustained oscillations has not been reported so far. An interesting question involves whether periodic reversal of the core polarity could occur through a sequence of outward spiralling trajectories and reversal events if steady-state gyration were maintained in a self-oscillatory system (Fig. 1c). This behaviour would be analogous to relaxation oscillations seen in threshold or integrate-and-fire oscillators, whereby energy is released discontinuously after the

[1]Institut d'Electronique Fondamentale, Université Paris-Sud, 91405 Orsay, France, [2]UMR 8622, CNRS, 91405 Orsay, France, [3]Unité Mixte de Physique CNRS/Thales and Université Paris-Sud, 1 avenue A. Fresnel, 91767 Palaiseau, France, [4]Department of Physics and Materials Science, City University of Hong Kong, Kowloon, Hong Kong, [5]Department of Solid State Sciences, Ghent University, Krijgslaan 281-S1, B-9000 Ghent, Belgium, [6]Department of Electrical Energy, Systems and Automation, Ghent University, Sint-Pietersnieuwstraat 41, B-9000 Ghent, Belgium. *e-mail: joo-von.kim@u-psud.fr.

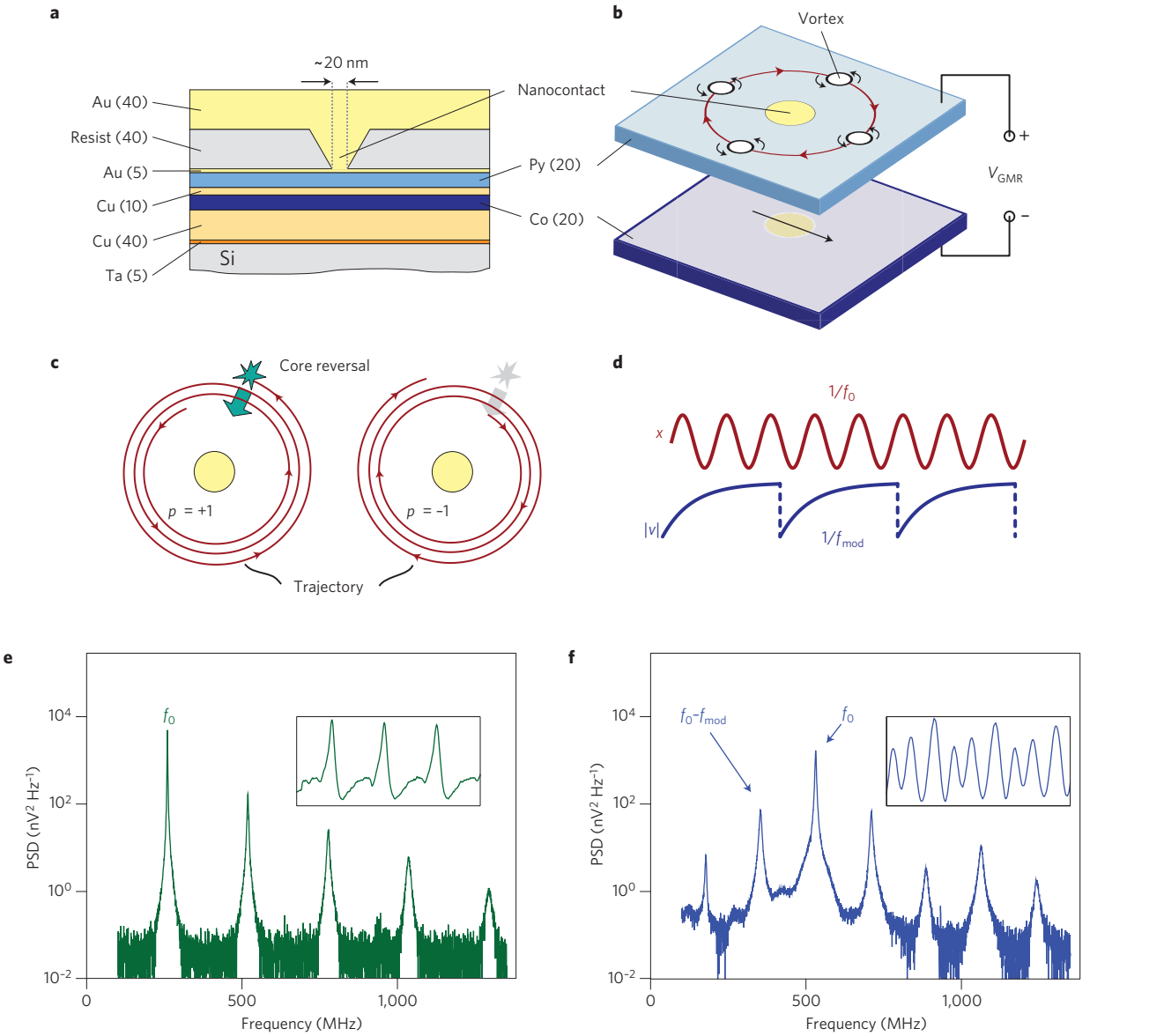


**Figure 1 | Schematic illustration of vortex dynamics in magnetic nanocontacts. a**, Multilayer composition of the pseudo spin valve studied, with numbers in parentheses indicating thicknesses in nanometres. **b**, Gyrotropic motion of the vortex in the permalloy (Py) layer, with uniform magnetization in the cobalt layer. A GMR signal arises from the variation of the relative magnetization orientations in the nanocontact area. **c**, Successive instances of vortex gyration and vortex core reversal. As the core spirals out from the nanocontact, its angular frequency decreases slightly but its linear velocity increases. When the critical velocity is reached, core reversal occurs, dissipating energy through spin waves, and the gyration restarts with an opposite sense of rotation. **d**, Schematic comparison of the periods for steady-state gyration and relaxation oscillations (periodic core reversal), highlighting the issue of commensurability. *x* represents the vortex core position and |*v*| the vortex speed. **e**,**f**, Measured power spectra and time traces (shown in inset) without (**e**) and with (**f**) relaxation oscillations.

system gradually charges and reaches a threshold value (see, for example, ref. 25). In the present case, relaxation oscillations would occur in the core velocity (Fig. 1d).

To elucidate the coexistence and possible interaction between the gyrotropic and relaxation modes, we studied vortex dynamics in the nanocontact system shown in Fig. 1a. It consists of a metallic point contact, fabricated using a nanoindentation technique with a conductive-tip atomic-force microscope[26], on a continuous film comprising a pseudo spin-valve multilayer composed of 20 nm of $Ni_{80}Fe_{20}$ alloy, 10 nm of Cu and 20 nm of Co. The cobalt layer is the reference layer and the permalloy layer is the free layer in which vortex dynamics takes place. Some representative voltage power spectra showing vortex dynamics are given in Fig. 1e,f. These spectra were obtained in a perpendicular applied field of $\mu_0 H = 13$ mT, following an initialization procedure (see Methods). Well-defined spectral peaks are seen, with the fundamental frequency $f_0$ well in the sub-gigahertz range. Two distinct behaviours are observed. In a low-current regime, the power spectrum comprises the fundamental with higher harmonics, where the power in each peak decreases with each higher harmonic (Fig. 1e). The time trace of the voltage oscillation in this regime (Fig. 1e inset) reveals a signal that is strongly non-sinusoidal, which suggests a non-circular orbit around the nanocontact. This behaviour has been observed in previous studies on nanocontact vortex oscillators[6,7]. In contrast, a modulation effect is seen for higher currents (Fig. 1f), whereby sidebands occur around the fundamental mode. This effect is also apparent in the time-domain traces, where a clear modulation in the signal amplitude can be seen (Fig. 1f inset).

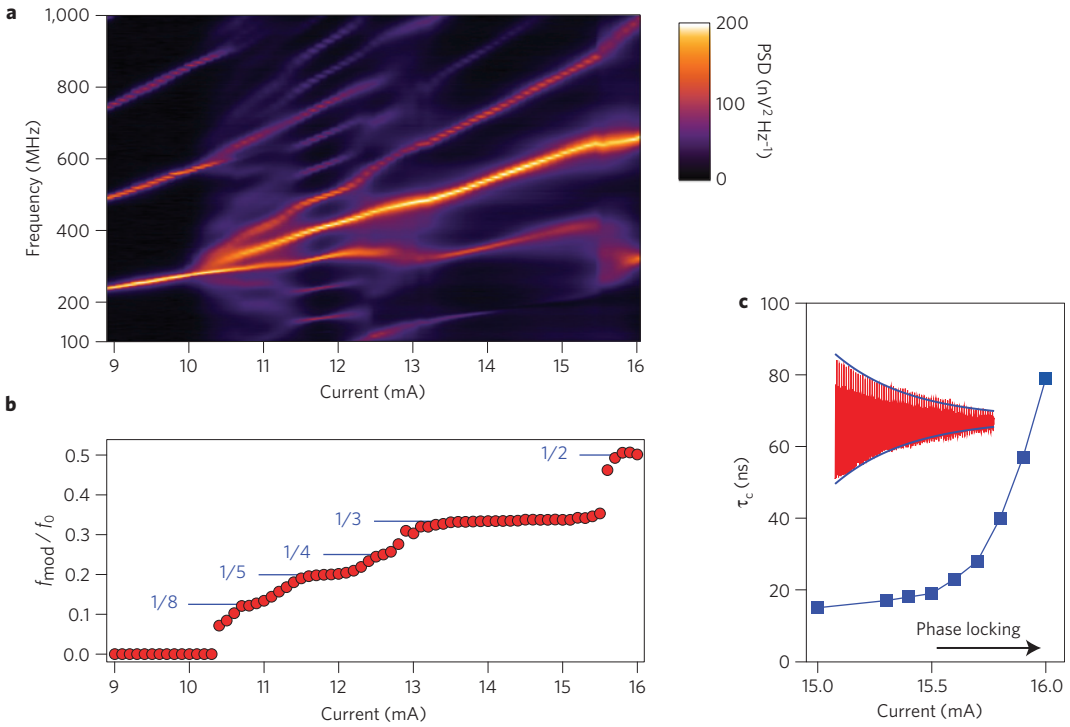


**Figure 2 | Experimental power spectrum of the nanocontact vortex oscillator. a**, Colour map of the PSD as a function of current, where modulation of the main frequency branch is visible with different modulation rates. **b**, Variation of the ratio between the modulation and central frequencies as a function of applied current, where plateaux indicate phase-locking between the gyration and modulation. **c**, Signal coherence time as a function of applied current around the $f_{mod}/f_0 = 1/2$ plateau, showing a strong improvement in coherence as the system is driven towards a phase-locked state.

We attribute this modulation to the periodic reversal of the vortex core, that is, relaxation oscillations. As the radius of vortex gyration remains almost constant in the low-current regime[27,28], core reversal first occurs (with increasing currents) when the angular frequency of gyration leads to a linear speed for the vortex core that reaches the critical value. For our experimental system, we identify an onset current of 10.3 mA at which relaxation oscillations, and therefore modulation sidebands, first occur. This can be seen in Fig. 2a, where the variation of the power spectrum with applied current, $I$, is represented as a colour map. Below this onset current, the fundamental frequency shows a quasi-linear variation with the applied current, as reported in previous work[6,7]. The region above 10.3 mA represents the behaviour reported here, where sidebands gradually fan out from the fundamental mode and settle into distinct branches at different current intervals.

To understand the origin of these branches, we plot the ratio between the modulation and central frequencies, $f_{mod}/f_0$, as a function of current in Fig. 2b. Above the onset current, $f_{mod}/f_0$ increases monotonically with current, but a number of plateaux occur at different current intervals. Clear plateaux are seen at $f_{mod} = f_0/5$, $f_{mod} = f_0/3$ and $f_{mod} = f_0/2$, at which large power is seen in the sidebands (Fig. 2a). Weaker plateaux are also seen at $f_{mod} = f_0/8$ and $f_{mod} = f_0/4$. These plateaux suggest a phase-locking phenomenon between the gyrotropic motion and the modulation. Outside the plateaux in $f_{mod}/f_0$ the sidebands fan out from the central peak, which corresponds to a modulation that is incommensurate with the central frequency, whereas at the plateaux the modulation frequency is locked to a specific fraction of the central frequency. As Fig. 2b shows, this locking persists over large intervals in which the central frequency is varied by a few hundred megahertz.

A key signature of phase-locking is the increased phase coherence of the oscillation signal in the phase-locked state. To confirm this, we focused on the current interval from 15 to 16 mA, that is, around the phase-locking plateau of $f_{mod} = f_0/2$, where we measured averaged time traces of the voltage oscillations. As these traces are proportional to the voltage autocorrelation function, the envelope of the averaged signal can be fitted with a decaying exponential, $\langle v(t)v(0)\rangle \sim \exp(-t/\tau_c)$, where the time constant $\tau_c$ is a direct measure of the signal coherence. The variation of this coherence time with current is given in Fig. 2c, with the inset showing a representative fit of the measured signal envelope to a decaying exponential. We observe a strong improvement in the coherence time as the system is gradually driven above $f_{mod} = f_0/3$ towards the $f_{mod} = f_0/2$ plateau with increasing current, as expected of a phase-locking phenomenon.

These modulation and phase-locking phenomena can be explained as follows. When the vortex reaches the critical velocity its polarity reverses, leading to a decrease in the orbital radius, as illustrated in Fig. 1c. The vortex then gyrates in the opposite sense until it attains the critical velocity again. The points at which core reversal takes place determine whether phase-locking occurs: if core reversal occurs after an integer number of orbital revolutions, then phase-locking occurs; otherwise, the modulation afforded by the periodic core reversal is incommensurate with the gyration frequency, resulting in modulation sidebands that fan out from the central frequency peak. The nature of the vortex orbit is therefore an important factor in determining the commensurability of the gyration and relaxation oscillation frequencies (Fig. 1d).

To explore this scenario in more detail, we performed micromagnetic simulations of the vortex dynamics in a magnetic nanocontact under the same conditions as those used in the experiment (see Methods and Supplementary Information). By following the same experimental procedure to nucleate vortex oscillations, we computed the map of the power spectral density (PSD) for the same current interval as studied in the experiment, which is shown in Fig. 3a. The results demonstrate a good quantitative agreement between the simulated and experimental

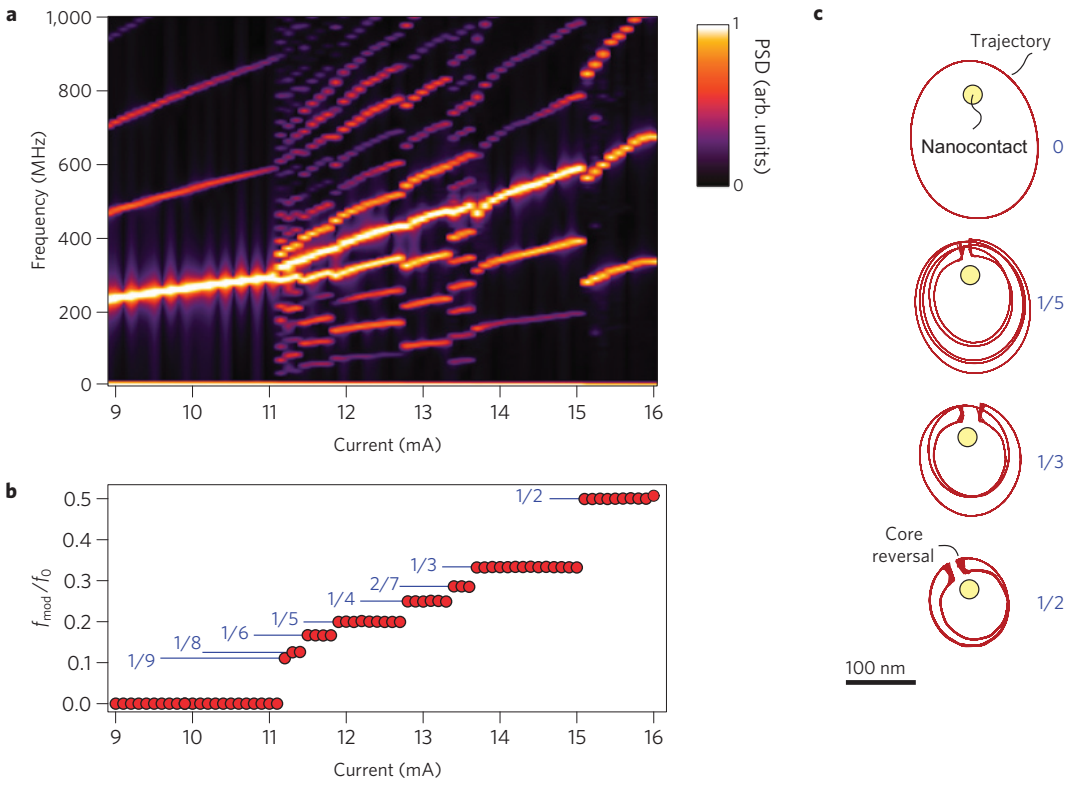


**Figure 3 | Calculated power spectra from micromagnetics simulations. a**, Colour map of the PSD as a function of current. **b**, Variation of the ratio between the modulation and central frequencies as a function of applied current, where plateaux indicate phase-locking between the gyration and modulation. **c**, Calculated vortex trajectories around the nanocontact for four different phase-locked regimes, with core-reversal events indicated.

frequencies, and confirm that the modulation originates from periodic core reversal, through sequences as shown in Fig. 1c. The current dependence of the calculated $f_{mod}/f_0$ ratio is given in Fig. 3b. The simulations reproduce all the experimentally observed locking ratios, with relatively good agreement on the current intervals at which they occur. There are also a number of locking ratios seen in the simulation that are absent in the experiment, notably, $f_{mod}/f_0 = 1/9$, 1/6, 2/7. The absence of these plateaux can be attributed either to thermal noise, because fluctuations in the vortex trajectories over long time scales result in incoherent modulation and broad sidebands in the power spectra[29], or to a difference between the experimental and simulated vortex trajectories.

The calculated vortex trajectories are presented in Fig. 3c. In the low-current regime an off-centred elliptical trajectory is found, with typical distances of 100–200 nm from the nanocontact, where the elongated shape results from the presence of a remnant antivortex created during the nucleation process. Although the antivortex is artificially pinned by the grid edge in the simulations, we contend that material defects will lead to similar pinning in the experimental system[30]. In any event, the proximity of the antivortex to the orbital dynamics is critical for describing the oscillation frequencies and phase-locking behaviour quantitatively, because pure circular orbits without an antivortex result in power spectra that differ qualitatively from the experimental data (see Supplementary Information). At higher currents (and consequently for faster vortex motion), the elliptical shape means that the critical velocity ($\sim$300 m s$^{-1}$) is first attained only at specific points along the orbit, as indicated by the jumps in the trajectories in Fig. 3c. These orbits shrink progressively with increasing currents owing to a corresponding increase in angular frequency of the orbital motion, which means that the critical velocity is attained for progressively smaller orbital radii. However, the points at which core reversal occurs only vary slightly with the current.

The modulation and phase-locking phenomena are a result of the competing frequencies (or periods) of the gyrotropic and relaxation oscillations (Fig. 1d). Analogous effects occur in other physical systems, for example, in the competing spatial periods of surface potentials and adatoms in the Frenkel–Kontorowa model[31], which fall into a broader class of phenomena involving commensurate–incommensurate phase transitions[32]. These are characterized by transitions between commensurate and incommensurate states, which are described by a winding number $\Omega$, representing the ratio between the competing frequencies present. Whether $\Omega$ is rational or irrational determines whether the state is commensurate or incommensurate, respectively. Here, we can associate $\Omega = f_{mod}/f_0$, with $\Omega(I)$ being referred to as a Devil's staircase[32]. As $\partial\Omega/\partial I = 0$ everywhere except at the steps between the plateaux, the staircase in Fig. 3b is referred to as a harmless staircase because transitions take place only between commensurate states, with no evidence of any incommensurate states present.

It is pertinent to enquire how the nature of the staircase changes if the perpendicular applied field, $H$, is varied, because the gyration frequency depends not only on its magnitude but also on how the core magnetization is oriented with respect to it, that is, on the sign of the core polarity $p$ (ref. 33). By varying the applied field, the ratio between the $p = +1$ and $p = -1$ orbital frequencies is also modified at constant current, which allows different values of $f_{mod}/f_0$ to be probed. The calculated staircases for three values of decreasing applied fields are presented in Fig. 4a. Whereas certain locking ratios remain present at all fields considered, incommensurate states occur as the field is reduced. Furthermore, the current intervals in which these states occur broaden at low fields, the most striking of which occurs between 13.9 and 14.7 mA in zero field. Note that $\partial\Omega/\partial I \neq 0$ for the incommensurate states, in contrast to the plateaux describing the commensurate (phase-locked) states, because the modulation due to relaxation oscillations

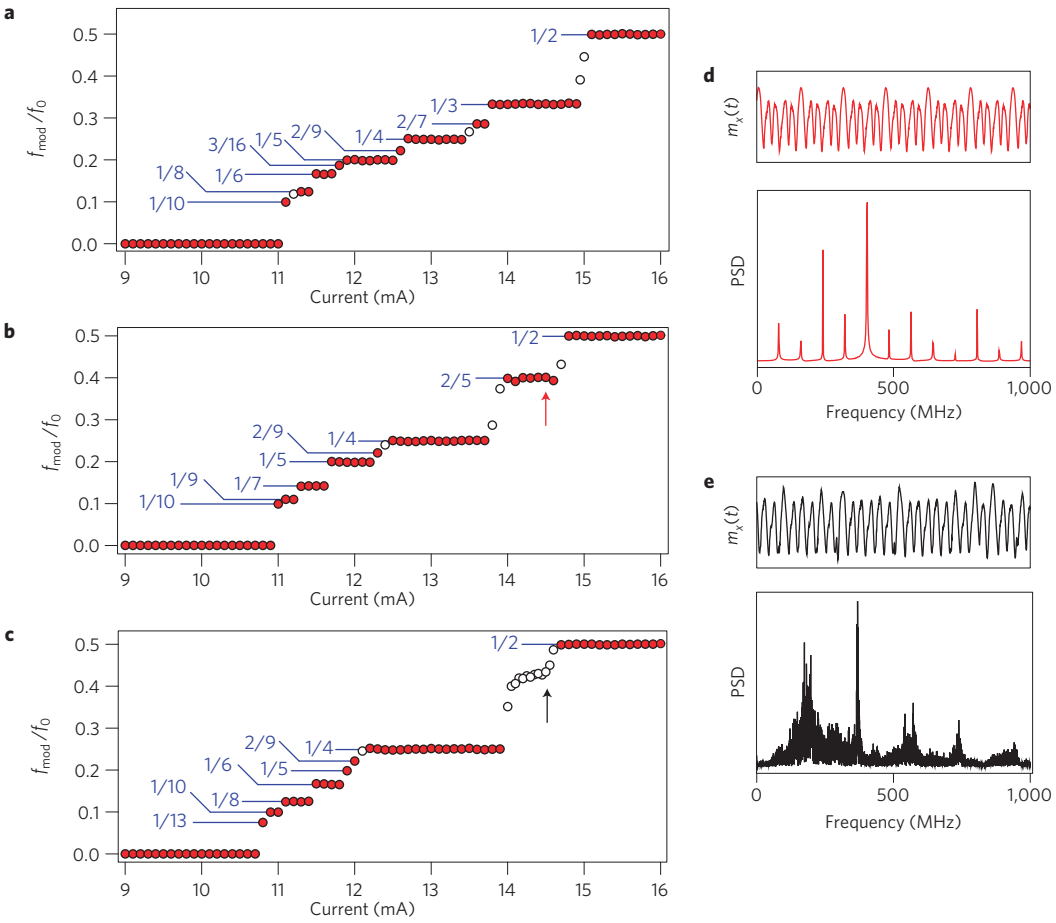


**Figure 4 | Simulated Devil's staircases and chaotic states. a**,**b**,**c**, The current-dependence of the winding number $f_{mod}/f_0$ for three applied perpendicular field values: $\mu_0 H = 10$ mT (**a**); $\mu_0 H = 5$ mT (**b**); $\mu_0 H = 0$ (**c**). Filled (red) circles denote commensurate states; open (white) circles denote incommensurate states. **d**,**e**, A sample time trace of one in-plane component of total magnetization, $m_x$, and its corresponding power spectrum for a commensurate state with $f_{mod}/f_0 = 2/5$ (**d**) and an incommensurate (chaotic) state with $f_{mod}/f_0 \approx 0.44432$ (**e**). The currents at which the spectra in **d** and **e** are taken are indicated by arrows in **b** and **c**, respectively.

can vary arbitrarily with respect to the gyration frequency. This is characteristic of an incomplete Devil's staircase.

To examine the nature of the incommensurate state, we compare the simulated time traces of a commensurate state of $f_{mod}/f_0 = 2/5$ under an applied field of $\mu_0 H = 5$ mT (Fig. 4d), with an incommensurate state of $f_{mod}/f_0 \approx 0.44432$ in zero field (Fig. 4e). As these two states occur at similar currents and fields, they involve similar dynamics. As the time trace in Fig. 4d shows, the commensurate state comprises a repeating motif of three $p = +1$ rotations followed by two $p = -1$ rotations, resulting in the locking ratio of 2/5. In stark contrast, the incommensurate state is characterized by waveforms with no clear repeating motifs. For example, the distinctly large oscillation that occurs every five periods in the $f_{mod}/f_0 = 2/5$ state (Fig. 4d) seems to be randomly distributed in the $f_{mod}/f_0 \approx 0.44432$ state (Fig. 4e). We verified that this behaviour persists up to 5 μs of simulation time and involves dynamics that is sensitive to initial conditions (see Supplementary Information). These are characteristic of a chaotic state, where discommensurations are randomly distributed with no noise present[32]. This point is well illustrated in the power spectra, which are given below each time trace in Fig. 4d,e. We observe narrow spectral peaks with well-defined sidebands for the commensurate case, where the spectral linewidth results only from the finite simulation time. In contrast, significant line broadening occurs for the incommensurate case, despite the theoretical frequency resolution of 500 kHz for the computed spectra. In the latter, line broadening results from an athermal noise, a key feature of temporal chaos.

This chaotic oscillation phase could find applications in secure communications. One possible scheme involves encryption through chaos, whereby the unpredictability stemming from the chaotic dynamics is used to bury information, resulting in a signal that would be perceived as noise by an eavesdropper[34]. For such schemes to work, the chaotic oscillators employed by the sender and the recipient need to be synchronized[35]. Although this aspect has not been investigated for the system presented here, it is known that similar magnetic vortex oscillators can phase-lock to driving currents[36,37]. We suggest that nanocontact vortex oscillators could provide an important system to realize such schemes, as they are agile[27,29] and operate at frequencies relevant for telecommunications. In this light, these nanoscale electrical oscillators could be useful for providing hardware-based encryption methods in mobile applications.

## Methods

The nanocontacts are fabricated on top of flat pseudo spin-valve multilayers with the composition Co (reference layer, 20 nm)/Cu (10 nm)/permalloy (free layer, 20 nm), with a nominal contact diameter of 20 nm following the methods described elsewhere[8]. The device and its series electrodes have a resistance of 20 Ω in the parallel state and a GMR of $\Delta R = 50$ mΩ. The coercivities of the free and reference layers are 0.5 mT and 1.3 mT, respectively. The pseudo spin valve is electrically shorted to an on-chip ground, and the nanocontact is connected to the coaxial cables through millimetre-long wire bonds. Experiments show that the

nanocontact can support applied currents of up to 16 mA without suffering any measurable degradation. All experiments performed on these samples therefore have an upper limiting current of 16 mA.

The vortex dynamics is inferred from the time-varying GMR signal of the entire spin-valve stack. The spectrum of the voltage oscillations was measured in the frequency domain with a spectrum analyser and in the time domain with a single-shot oscilloscope[38]. All measurements were performed at room temperature. For signal averaging, the trigger condition was applied after frequency filtering to isolate the spectral line of lowest frequency in the signal.

To initiate the vortex oscillations in the experiment, a current of 16 mA was first applied to the nanocontact. This represents typically the largest current that can be applied without damaging the nanocontact studied, but is insufficient to directly promote vortex nucleation in the permalloy layer[39]. Next, a large in-plane field was applied to saturate the free-layer magnetization along one direction, and the field was then slowly ramped down to zero and reversed. When the applied field crossed the coercive field of the permalloy layer, we observed large peaks in the power spectrum of the voltage signal, with central frequencies in the range of a few hundred megahertz; these peaks are attributed to the gyrotropic motion of a vortex around the nanocontact. In this scenario, at the moment the magnetization reverses, a domain wall sweeps across the nanocontact area and a vortex-like structure is captured by the Zeeman energy potential, associated with the Oersted–Ampère field generated by the current. The power spectra were then acquired for decreasing currents from the initial value of 16 mA in a magnetic field of 13 mT, applied perpendicularly to the film plane. No hysteresis in the power spectra was seen for increasing currents.

The micromagnetic simulations consist of solving the Landau–Lifshitz equation of motion for the dynamics of the permalloy free layer at zero temperature, with Gilbert damping and in-plane spin-torque terms, using the software package MuMax[40]. The simulated region is square and has dimensions of $1{,}280 \times 1{,}280 \times 20$ nm, discretized with $512 \times 512 \times 1$ identical finite difference cells. For the material parameters, we used a saturation magnetization ($M_s$) of 800 kA m$^{-1}$, an exchange constant ($A$) of 10 pJ m$^{-1}$, a Gilbert damping constant ($\alpha$) of 0.013 and a spin polarization ($P$) of 0.5. For a subset of the applied currents studied, we verified that discretizing along the film thickness using 2.5-nm-thick cells (with $512 \times 512 \times 8$ finite difference cells) led to the same dynamics. To simplify the problem, we neglected the non-adiabatic spin-torque term for all the simulations presented here. However, we have checked that its inclusion (using realistic values of $\beta$) did not lead to any significant differences for the oscillation frequencies, as expected from theory[28]. The spatial distributions of the applied current and its associated Oersted–Ampère field were computed using a finite-element method[15], and were subsequently integrated into the micromagnetics simulations.

Received 22 March 2012; accepted 13 June 2012; published online 8 July 2012

## References


1. Hubert, A. & Schäfer, R. *Magnetic Domains* (Springer, 1998).
2. Choe, S. B. Vortex core-driven magnetization dynamics. *Science* **304,** 420–422 (2004).
3. Buchanan, K. S. *et al.* Soliton-pair dynamics in patterned ferromagnetic ellipses. *Nature Phys.* **1,** 172–176 (2005).
4. Novosad, V. *et al.* Magnetic vortex resonance in patterned ferromagnetic dots. *Phys. Rev. B* **72,** 024455 (2005).
5. Yamada, K. *et al.* Electrical switching of the vortex core in a magnetic disk. *Nature Mater.* **6,** 270–273 (2007).
6. Pufall, M., Rippard, W., Schneider, M. & Russek, S. Low-field current-hysteretic oscillations in spin-transfer nanocontacts. *Phys. Rev. B* **75,** 140404 (2007).
7. Mistral, Q. *et al.* Current-driven vortex oscillations in metallic nanocontacts. *Phys. Rev. Lett.* **100,** 257201 (2008).
8. Ruotolo, A. *et al.* Phase-locking of magnetic vortices mediated by antivortices. *Nature Nanotech.* **4,** 528–532 (2009).
9. Pribiag, V. S. *et al.* Magnetic vortex oscillator driven by d.c. spin-polarized current. *Nature Phys.* **3,** 498–503 (2007).
10. Dussaux, A. *et al.* Large microwave generation from current-driven magnetic vortex oscillators in magnetic tunnel junctions. *Nature Commun.* **1,** 8 (2010).
11. Slonczewski, J. C. Current-driven excitation of magnetic multilayers. *J. Magn. Magn. Mater.* **159,** L1–L7 (1996).
12. Berger, L. Emission of spin waves by a magnetic multilayer traversed by a current. *Phys. Rev. B* **54,** 9353–9358 (1996).
13. Berger, L. Exchange interaction between ferromagnetic domain wall and electric current in very thin metallic films. *J. Appl. Phys.* **55,** 1954–1956 (1984).
14. Zhang, S. & Li, Z. Roles of nonequilibrium conduction electrons on the magnetization dynamics of ferromagnets. *Phys. Rev. Lett.* **93,** 127204 (2004).
15. Petit-Watelot, S., Otxoa, R. M. & Manfrini, M. Electrical properties of magnetic nanocontact devices computed using finite-element simulations. *Appl. Phys. Lett.* **100,** 083507 (2012).
16. Sheka, D. D., Gaididei, Y. & Mertens, F. G. Current induced switching of vortex polarity in magnetic nanodisks. *Appl. Phys. Lett.* **91,** 082509 (2007).
17. Guslienko, K., Lee, K-S. & Kim, S-K. Dynamic origin of vortex core switching in soft magnetic nanodots. *Phys. Rev. Lett.* **100,** 027203 (2008).
18. Hertel, R. & Schneider, C. Exchange explosions: Magnetization dynamics during vortex-antivortex annihilation. *Phys. Rev. Lett.* **97,** 177202 (2006).
19. Gouvea, M. E., Wysin, G. M., Bishop, A. R. & Mertens, F. G. Vortices in the classical two-dimensional anisotropic Heisenberg model. *Phys. Rev. B* **39,** 11840–11849 (1989).
20. Vansteenkiste, A. *et al.* X-ray imaging of the dynamic magnetic vortex core deformation. *Nature Phys.* **5,** 332–334 (2009).
21. Kravchuk, V. P., Sheka, D. D., Mertens, F. G. & Gaididei, Y. Off-centred immobile magnetic vortex under influence of spin-transfer torque. *J. Phys. D* **44,** 285001 (2011).
22. Van Waeyenberge, B. *et al.* Magnetic vortex core reversal by excitation with short bursts of an alternating field. *Nature* **444,** 461–464 (2006).
23. Pigeau, B. *et al.* Optimal control of vortex-core polarity by resonant microwave pulses. *Nature Phys.* **7,** 26–31 (2010).
24. Kammerer, M. *et al.* Magnetic vortex core reversal by excitation of spin waves. *Nature Commun.* **2,** 279–276 (2011).
25. Pikovsky, A., Rosenblum, M. & Kurths, J. *Synchronization: A Universal Concept in Nonlinear Sciences* (Cambridge Univ. Press, 2001).
26. Bouzehouane, K. *et al.* Nanolithography based on real-time electrically controlled indentation with an atomic force microscope for nanocontact elaboration. *Nano Lett.* **3,** 1599–1602 (2003).
27. Manfrini, M. *et al.* Agility of vortex-based nanocontact spin torque oscillators. *Appl. Phys. Lett.* **95,** 192507 (2009).
28. Kim, J-V. & Devolder, T. Theory of the power spectrum of spin-torque nanocontact vortex oscillators. Preprint at http://arxiv.org/abs/1007.3859 (2010).
29. Manfrini, M. *et al.* Frequency shift keying in vortex-based spin torque oscillators. *J. Appl. Phys.* **109,** 083940 (2011).
30. Compton, R. & Crowell, P. Dynamics of a pinned magnetic vortex. *Phys. Rev. Lett.* **97,** 137202 (2006).
31. Chaikin, P. M. & Lubensky, T. C. *Principles of Condensed Matter Physics* (Cambridge Univ. Press, 1995).
32. Bak, P. Commensurate phases, incommensurate phases and the devil's staircase. *Rep. Prog. Phys.* **45,** 587 (1982).
33. De Loubens, G. *et al.* Bistability of vortex core dynamics in a single perpendicularly magnetized nanodisk. *Phys. Rev. Lett.* **102,** 177602 (2009).
34. Cuomo, K. M. & Oppenheim, A. V. Circuit implementation of synchronized chaos with applications to communications. *Phys. Rev. Lett.* **71,** 65–68 (1993).
35. Pecora, L. M. & Carroll, T. L. Synchronization in chaotic systems. *Phys. Rev. Lett.* **64,** 821–824 (1990).
36. Lehndorff, R., Bürgler, D. E., Schneider, C. M. & Celinski, Z. Injection locking of the gyrotropic vortex motion in a nanopillar. *Appl. Phys. Lett.* **97,** 142503 (2010).
37. Dussaux, A. *et al.* Phase locking of vortex based spin transfer oscillators to a microwave current. *Appl. Phys. Lett.* **98,** 132506 (2011).
38. Devolder, T. *et al.* Time-resolved zero field vortex oscillations in point contacts. *Appl. Phys. Lett.* **95,** 012507 (2009).
39. Devolder, T. *et al.* Vortex nucleation in spin-torque nanocontact oscillators. *Appl. Phys. Lett.* **97,** 072512 (2010).
40. Vansteenkiste, A. & Van de Wiele, B. MuMax: A new high-performance micromagnetic simulation tool. *J. Magn. Magn. Mater.* **323,** 2585–2591 (2011).


## Acknowledgements

This work was partially supported by the European Commission, under contract numbers MRTN-CT-2006-035327 SPINSWITCH and MRTN-CT-2008-215368-2 SEMISPINNET, the French National Research Agency (ANR), within the VOICE project no ANR-09-NANO-006, the RTRA foundation 'Triangle de la Physique', under contract number 2007-051T, and the Flanders Research Foundation. The authors thank R. Guillemet, S. Fusil and C. Deranlot for their assistance during the growth and fabrication of the samples, and A. Dussaux for complementary experiments and discussions.

## Author contributions

J-V.K., T.D., A.R., J.G. and V.C. designed the project, and V.C., T.D. and J-V.K. coordinated the project. K.B. fabricated the samples. T.D. designed and implemented the experimental set-up. A.R. and T.D. performed the high-frequency electrical measurements. T.D., A.R. and J-V.K. analysed the data. S.P-W., J-V.K., R.M.O. and T.D. interpreted the data and developed the model. A.V. and B.V.d.W. wrote the micromagnetics simulation code. J-V.K., S.P-W. and R.M.O. performed the simulations and interpreted the results. J-V.K. prepared the manuscript. All authors edited and commented on the manuscript.

## Additional information

The authors declare no competing financial interests. Supplementary information accompanies this paper on www.nature.com/naturephysics. Reprints and permissions information is available online at www.nature.com/reprints. Correspondence and requests for materials should be addressed to J-V.K.